Influences of pH and substrate supply on the ratio of iron to sulfate reduction

Running head: Controls on the ratio of iron to sulfate reduction

Janet M. Paper[1,6], Theodore M. Flynn[2,7], Maxim I. Boyanov[2,3], Kenneth M. Kemner[2], Ben R. Haller[1,8], Kathleen Crank[4], AnneMarie Lower[4], Qusheng Jin[5], Matthew F. Kirk[1*]

[1]Department of Geology, Kansas State University, Manhattan, KS 66506, USA

[2]Biosciences Division, Argonne National Laboratory, Argonne, IL 60439, USA

[3]Bulgarian Academy of Sciences, Institute of Chemical Engineering, Sofia, 1113, Bulgaria

[4]Department of Biology, Benedictine College, Atchison, KS 66002, USA

[5]Department of Earth Sciences, University of Oregon, Eugene 97403, OR

[6]Current address: Department of Biology, Benedictine College, Atchison, KS 66002, USA

[7]Current address: California Department of Water Resources, Sacramento, CA 95814, USA

[8]Current address: Kansas Department of Health and Environment, Topeka, KS 66612, USA

*Correspondence: mfkirk@ksu.edu, 785-532-6724

ACKNOWLEDGEMENTS

This project was supported by funding from NSF awards EAR-1753436 and EPS-0903806, the Benedictine Discovery Day Program, and the State of Kansas through the Kansas Board of Regents. The XAFS data collection and analyses and effort of KMK, MIB, and TMF were supported by the Argonne Wetlands Hydrobiogeochemistry Scientific Focus Area (SFA) at Argonne National Laboratory funded by the Subsurface Biogeochemical Research Program,

Office of Biological and Environmental Research, Office of Science, U.S. Department of Energy (DOE), under contract DE-AC02-06CH11357. MRCAT/EnviroCAT operations are supported by DOE and the MRCAT/EnviroCAT member institutions. This research used resources of the Advanced Photon Source, a U.S. DOE Office of Science User Facility operated for the DOE Office of Science by Argonne National Laboratory under Contract No. DE-AC02-06CH11357.

Abstract

Iron reduction and sulfate reduction often occur simultaneously in anoxic systems, and where that is the case, the molar ratio between the reactions (i.e., Fe/SO_4^{2-} reduced) influences their impact on water quality and carbon storage. Previous research has shown that pH and the supply of electron donors and acceptors affect that ratio, but it is unclear how their influences compare and affect one another. This study examines impacts of pH and the supply of acetate, sulfate, and goethite on the ratio of iron to sulfate reduction in semi-continuous sediment bioreactors. We examined which parameter had the greatest impact on that ratio and whether the parameter influences depended on the state of each other. Results show that pH had a greater influence than acetate supply on the ratio of iron to sulfate reduction, and that the impact of acetate supply on the ratio depended on pH. In acidic reactors (pH 6.0 media), the ratio of iron to sulfate reduction decreased from 3:1 to 2:1 as acetate supply increased (0 to 1 mM). In alkaline reactors (pH 7.5 media), iron and sulfate were reduced in equal proportions, regardless of acetate supply. Secondly, a comparison of experiments with and without sulfate shows that the extent of iron reduction was greater if sulfate reduction was occurring and that the effect was larger in alkaline reactors than acidic reactors. Thus, the influence of sulfate supply on iron reduction extent also depended on pH and suggests that iron reduction grows more dependent on sulfate reduction as

pH increases. Our results compare well to trends in groundwater geochemistry and provide further evidence that pH is a major control on iron and sulfate reduction in systems with crystalline (oxyhydr)oxides. pH not only affects the ratio between the reactions but also the influences of other parameters on that ratio.

Summary statement: This study uses bioreactor experiments to examine environmental controls on the ratio of iron reduction to sulfate reduction. Findings underscore the importance of pH as a major control on the relationship between the reactions. pH not only affected the ratio between the reactions but also influences of other parameters on that ratio. Moreover, the results suggest that iron reduction grows increasingly dependent on sulfate reduction as pH increases.

Key words: iron reduction, sulfate reduction, anoxic environments, *Geobacter*, goethite

1. INTRODUCTION

Iron reduction and sulfate reduction help drive organic carbon oxidation in anoxic environments and in doing so impact water quality, nutrient availability, and carbon storage (Jorgensen, 1982; Roden & Edmonds, 1997; Borch *et al.*, 2010; Kirk *et al.*, 2013; Muller *et al.*, 2017). The nature of that impact depends in part on the molar ratio between the reactions (i.e., Fe/SO_4^{2-} reduced). Where the reactions occur independently, their products (ferrous iron (Fe(II)) and sulfide) can accumulate in solution and degrade water quality (Chapelle & Lovley, 1992; Rabus *et al.*, 2006). In contrast, where the reactions occur simultaneously, their products can precipitate as mackinawite (~FeS) (Berner, 1970; Luther & Rickard, 2005; Michel *et al.*, 2005), which can ultimately transform into greigite and pyrite (Hunger & Benning, 2007). In

environments hosting both reactions, accumulation of dissolved ferrous iron and sulfide varies with the ratio of iron reduction and sulfate reduction (Chapelle *et al.*, 2009). That ratio is known to be sensitive to pH and the supply of energy resources for microbial metabolism, but the relative influences of those variables are unclear. By learning more about these controls, we will be better able to use them to interpret and manage the biogeochemistry of anoxic systems.

Iron and sulfate reduction are mediated by microorganisms in low-temperature (i.e., surficial) systems. Numerous groups of microorganisms are capable of reducing sulfate for dissimilatory and assimilatory metabolism (Muyzer & Stams, 2008; Anantharaman *et al.*, 2018). Similarly, a wide diversity of microorganisms can catalyze iron reduction for dissimilatory metabolism (Lovley & Phillips, 1988; Weber *et al.*, 2006). In addition, iron can also be reduced abiotically by reaction with sulfide and reduced humic substances generated by microbial activity (Pyzik & Sommer, 1981; Canfield, 1989; Lovley *et al.*, 1996; Roden *et al.*, 2010).

Multiple lines of evidence have shown that the ratio of iron reduction to sulfate reduction decreases as pH increases in anoxic systems. Results from previous studies that identify this relationship include rates observed in an aquifer (Jakobsen & Postma, 1999), findings from culturing experiments (Küsel & Dorsch, 2000; Kirk *et al.*, 2013; Flynn *et al.*, 2014), and variation in groundwater geochemistry in U.S. aquifers (Kirk *et al.*, 2016).

One potential reason for this relationship is that pH has a stronger influence on the free energy yield of iron reduction than sulfate reduction (Postma & Jakobsen, 1996; Bethke *et al.*, 2011; Jin & Kirk, 2018a). Oxidized iron in soil and sediment most commonly exists within a solid phase, such as a ferric oxide, oxyhydroxide, or hydroxide solid (Cornell & Schwertmann, 2003). Hereafter, we refer to these phases collectively as (oxyhydr)oxides. Where those phases are reductively dissolved, the reaction consumes a large number of protons, as shown in the

example reaction, which includes acetate (CH_3COO^-) as the electron donor and goethite (FeOOH) as a source of ferric iron (Fe(III)):

$$CH_3COO^- + 8\,FeOOH(s) + 15\,H^+ \leftrightarrow 2\,HCO_3^- + 8\,Fe^{2+} + 12\,H_2O \quad (1)$$

In contrast, sulfate reduction coupled with acetate oxidation consumes at most one proton:

$$CH_3COO^- + SO_4^{2-} + H^+ \leftrightarrow 2\,HCO_3^- + H_2S(aq) \quad (2)$$

Therefore, as pH increases, the Gibbs free energy yield of sulfate reduction varies little whereas the free energy yield of iron reduction decreases rapidly (Postma & Jakobsen, 1996; Bethke *et al.*, 2011; Jin & Kirk, 2018a). This difference can impact the ratio of iron reduction to sulfate reduction by affecting iron reduction kinetics. Microbial reactions that release more energy can have kinetic advantages over those releasing less energy (Jin & Bethke, 2007; Jin, 2012; LaRowe *et al.*, 2012; LaRowe & Amend, 2015; Jin & Kirk, 2018b). As such, the rate of iron reduction may decrease in response to decreasing energy yield with increasing pH.

Another potential reason pH influences the ratio of iron to sulfate reduction is that pH affects ferrous iron sorption. In general, ferrous iron is more soluble than ferric iron in solutions at near-neutral pH (Stumm & Morgan, 1996), and thus dissolved ferrous iron can accumulate during iron reduction (equation 1). However, some portion of the ferrous iron produced can also sorb onto the residual ferric (oxyhydr)oxide mineral:

$$\equiv FeOH + Fe^{2+} \leftrightarrow \equiv FeOFe^+ + H^+ \quad (3)$$

where $\equiv FeOH$ and $\equiv FeOFe^{+}$ represent uncomplexed and complexed sorbing sites on goethite, respectively (Dixit & Hering, 2006). Because the reaction produces a proton, ferrous iron sorption becomes more favorable as pH increases (Dixit & Hering, 2006). Sorption of ferrous iron fouls (oxyhydr)oxide surfaces and causes the rate of iron reduction to decrease (Roden & Urrutia, 1999; Urrutia *et al.*, 1999; Benner *et al.*, 2002). Thus, as pH increases, iron reduction may be more likely to slow in response to increasing ferrous iron sorption.

In addition to pH, electron donor supply also has the potential to influence the ratio of iron reduction to sulfate reduction. Because ferric iron typically exists within a solid phase, the surface area of the solid can limit the rate of electron transfer to ferric iron (Roden & Zachara, 1996; Roden, 2003, 2006). Where the rate of electron donor supply exceeds that limit, we reason that excess electron donor may divert to alternative reactions, such as sulfate reduction, even if iron reduction is favored otherwise. More generally, previous studies have shown that microbial reactions can coexist when electron donor supply is not limiting (Lovley & Phillips, 1987; Lovley & Goodwin, 1988; Achtnich *et al.*, 1995; Küsel & Dorsch, 2000).

Lastly, electron acceptor supply helps determine if the reactions can occur simultaneously. For both reactions to occur within the same environment, a source of ferric iron and sulfate must be available. Beyond that basic requirement, ferric iron source also has the potential to influence the ratio of iron to sulfate reduction. Ferric (oxyhydr)oxide reactivity varies widely, reflecting variation in mineral properties as well as environmental conditions (Konhauser *et al.*, 2011). In general, however, poorly crystalline phases such as ferrihydrite (~$Fe(OH)_3$) tend to have higher surface areas and solubilities than more stable phases, such as goethite and hematite (Fe_2O_3). Iron reduction rates have been found to increase with (oxyhdr)oxide surface

area and solubility (Larsen & Postma, 2001; Roden, 2003, 2006; Bonneville *et al.*, 2004, 2009; Cutting *et al.*, 2009). Therefore, environments with poorly crystalline phases may tend to have higher ratios of iron to sulfate reduction than those with highly crystalline phases.

These previous studies provide insight into the roles of pH and supply of electron donors and acceptors as environmental factors that influence the ratio of iron to sulfate reduction. However, it remains unclear which of these environmental factors has the biggest influence on the reaction ratio. Furthermore, it is also unclear whether there are interaction effects between these factors. For example, does the influence of electron donor supply on the ratio of iron to sulfate reduction depend on the pH of the environment?

To help answer these questions, we carried out semi-continuous bioreactor experiments that examined variation in pH alongside variation in electron donor concentration. We included bioreactors with goethite as a source of ferric iron and acetate as an electron donor, as well as control reactors that lacked sulfate and goethite. We inoculated all of the bioreactors with marsh sediment that included a natural microbial consortium capable of iron and sulfate reduction. Lastly, to test the environmental relevance of our experiments, we compare our results to broad spatial-scale trends in the chemistry of groundwater from U.S. aquifers.

2. MATERIALS AND METHODS

2.1. Study design

We performed five experiments in triplicate, each consisting of two sets of semi-continuous bioreactors: one that received acidic medium (pH 6.0) and one that received alkaline medium (pH 7.5) (Table 1). In our experiment labels, S stands for sulfate, NA, LA, and HA indicate no acetate, low acetate, and high acetate, respectively, and NFe indicates no iron. Media

for experiments S-NA, S-LA, S-HA included 0, 0.25, and 1 mM acetate, respectively, and 1.5 - 2.5 mM sulfate, allowing us to test the influence of acetate flux on the balance between iron reduction and sulfate reduction. Experiment HA was identical to S-HA, except no sulfate was included in the media. Similarly, experiment S-LA-NFe was similar to S-LA, except we did not add goethite to the reactor sediment. Thus, HA and S-LA-NFe represent sulfate and ferric iron control experiments, respectively. Lastly, we inoculated all of the reactors with the same marsh sediment, which was previously analyzed for chemical and microbial compositions, as described below (section 2.4).

We selected the pH range of the media for two reasons. First, that pH range is common in natural systems hosting iron and sulfate reduction. For example, Kirk et al. (2016), analyzed the chemistry of groundwater from zones of iron and/or sulfate reduction in 19 aquifers distributed across the U.S. and found that more than 50% of the >5,000 samples in their dataset had pH between 6.0 and 7.5 (Table SI12). Secondly, thermodynamic calculations show that goethite reduction can be favored over sulfate reduction at acidic pH but that sulfate reduction is favored above pH 6.5-7.0 (Jin & Kirk, 2018a). Thus, our experiments consider both sides of that tipping point.

2.2. Aqueous media preparation

We defined the composition of aqueous media for the bioreactor experiments based on the composition of the water overlying the marsh sediment and included small amounts of ammonium (50 μM) and phosphate (1 μM) to stimulate microbial activity (Table 1). We made media solutions in volumetric flasks and dispensed them into 1 L solution bottles sealed with either rubber stoppers or ported PTFE solution bottle caps. To remove oxygen and set the pH of

185 the medium, we sparged the media for 2 hr/L with oxygen-free gas flowing at >0.5 L/min and
186 composed of CO_2 and N_2. We set the pH to either 6.0 or 7.5 by adjusting the N_2:CO_2 ratio of the
187 sparge gas. The N_2:CO_2 ratio of the sparge gas was 65:35 for pH 6.0 media and 99:1 for pH 7.5
188 media. We scrubbed trace oxygen from the gas by passing it through a heated column filled with
189 copper wool (Hungate, 1969). We measured the pH of the media each week and, if it deviated
190 from target values, we re-sparged the medium.
191
192 **2.3. Bioreactors**
193 The bioreactors consisted of 160 mL serum bottles that contained 100 mL of aqueous
194 medium, 1 g of wet marsh sediment inoculum, and except for S-LA-NFe reactors, 1 mmol of
195 goethite (i.e., 10 mmol/L). We synthesized the goethite by slowly oxidizing a bicarbonate-
196 buffered solution of ferrous chloride as described by Schwertmann and Cornell (2000) and
197 verified its identity prior to its initial use using X-ray diffraction (XRD) and high-resolution
198 transmission electron microscopy (HR-TEM) (Kirk *et al.*, 2010). Prior to this study, we
199 reanalyzed the goethite again using X-ray absorption spectroscopy (XAS), as described
200 previously (Marquart *et al.*, 2019). Results of the XAS analyses indicate that the synthetic
201 goethite was mostly goethite (75%) mixed with a disordered iron phase (ferrihydrite) or possibly
202 nano-goethite crystals (Marquart *et al.*, 2019) (Fig. SI1). For simplicity we refer to the synthetic
203 goethite simply as "goethite", but we acknowledge the possibility that a portion of the ferric
204 mineral was ferrihydrite.
205 We assembled the bioreactors as described by Marquart et al. (2019). We added aqueous
206 medium and goethite, sparged the bioreactors with N_2, plugged them with butyl rubber stoppers,
207 and then sterilized them with an autoclave (30 minutes at 121°C). Next, we placed the

bioreactors in an anaerobic chamber (Coy Labs, 2-5% H_2 with N_2 balance and Pd catalyst), removed their stoppers, and inoculated them with marsh sediment. We homogenized the marsh sediment and measured the exact mass added to each reactor. We also added ferrous chloride (100 μM final concentration) to consume trace oxygen that may have been present after reactor assembly. Next, we replaced the stoppers and sealed the reactors with aluminum crimp seals, inserted a sterile 4-inch stainless steel needle through the stopper, and capped the needle with a syringe valve. The needle terminated in the aqueous phase of the reactors at a level about 2 cm above the bottom and was used to add and remove fluid during the incubation. Lastly, we removed the reactors from the anaerobic chamber and sparged them with filter-sterilized, O_2-free gas to adjust the proportion of N_2 and CO_2 gas according to Table 1.

The reactors incubated in the dark at 20°C until acetate concentrations were stable for >1 month (91 days total). Every seven days during the incubation, we removed 1/5 of the aqueous volume from each reactor (i.e., 20 mL) without removing reactor solids. Then, immediately afterward, we replaced the sampled volume with fresh medium and gently swirled the reactors to mix them. We chemically analyzed the volume removed using the techniques described below. This semi-continuous sediment bioreactor approach is similar to an aquifer, in that sulfate and other solutes migrate with flowing groundwater and sources of ferric iron exist within the solid matrix.

2.4. Marsh sediment inoculum

We collected marsh sediment for the reactors from the floodplain of the Big Blue River near its mouth on Tuttle Creek Reservoir (latitude 039°27’38.988”N longitude 096°41’25.3428”W). The site was chosen because it is conveniently located near Kansas State

University (site of the experiments) and because diverse communities of anaerobic microorganisms are common in wetland sediments (Pester *et al.*, 2012; Kim & Liesack, 2015). We collected samples on January 30, 2016. At the time, the sediment was submerged beneath ice and about 0.25 m of water. We collected water-saturated soil samples for inoculum in a sterile (autoclaved; 121°C for 30 min) jar and stored them at 20°C in the laboratory for 6 months before starting the experiments. This pre-incubation period allowed endogenous electron donors (e.g., organic matter) to partially deplete before we started the experiments.

In addition to the inoculum sample, we also collected soil samples for chemical and microbiological analysis and water samples for chemical analysis. We stored the soil samples in sterile 50 mL centrifuge tubes at −80°C and the water samples in 60 mL polyethylene bottles at 4°C. We characterized the pH, elemental composition, organic matter content, particle size distribution, mineralogy, and microbial community composition of the sediment. Results of the analyses are presented in Marquart et al. (2019). To briefly summarize, those analyses showed that the sediment was primarily composed of clay minerals with 0.7 mmol Fe and 7.5 mmol organic carbon per gram. XAS analysis indicates that the iron in the sediment was ferric iron and that it existed primarily within clay minerals (Fig. SI2; Table SI2). Microbial community analysis reveals a diverse community that includes groups commonly associated with iron reduction and sulfate reduction, including *Geobacter* and members of the order *Desulfobacterales* (Table SI9).

2.5. Chemical Analysis

2.5.1. Analysis of water and gas samples

253 We monitored the chemistry of reactor solutions and gas to identify variation in the
254 reaction ratio. Each week during the incubation, we measured pH and concentrations of anions
255 (acetate, chloride, and sulfate) and total dissolved sulfide and ferrous iron in reactor effluent
256 samples. We also periodically analyzed headspace methane abundance and effluent
257 concentrations of cations (sodium, potassium, magnesium, and calcium) and alkalinity.
258 Similarly, we analyzed pH, alkalinity, and concentrations of anions and cations in the marsh
259 water sample and each batch of aqueous medium.
260 For all water chemistry analyses except pH measurements, we filtered the samples using
261 syringe filters with 0.45 μm pores. We measured pH using an Oakton PC-300 pH meter. To
262 measure ferrous iron and sulfide concentrations, we used the ferrozine method (Stookey, 1970)
263 and the methylene blue method (Eaton *et al.*, 1995), respectively, with a Thermo Scientific
264 Genesys 10S UV-Vis spectrophotometer. We analyzed alkalinity concentrations using Gran
265 alkalinity titrations with 0.02 N sulfuric acid. To measure anion and cation concentrations, we
266 used Dionex ICS-1100 ion chromatographs. For methane analysis, we used a GOW MAC series
267 580 gas chromatograph with a thermal conductivity detector. Prior to extracting gas samples, we
268 measured the headspace pressure using a low-pressure mechanical gauge. Uncertainty and
269 detection limit values for our water and gas chemistry methods are available in Table SI1.
270
271 *2.5.2. Analysis of sediment samples*
272 We evaluated the abundance of ferrous iron in subsamples of homogenized reactor
273 sediment at the end of the experiment by measuring 0.5 N HCl extractable ferrous iron (Heron *et*
274 *al.*, 1994). The approach provides an estimate of the abundance of labile ferrous iron, including
275 sorbed ferrous iron and ferrous iron in siderite ($FeCO_3$) and mackinawite (FeS). To evaluate

276 speciation of iron in the solid phase of select reactors at the end of the experiment, we used iron
277 K-edge (7,112 eV) XAS measurements at the MR-CAT/EnviroCAT bending magnet beamline
278 (Sector 10, Advanced Photon Source, Argonne National Laboratory) (Kropf *et al.*, 2010). For the
279 analysis, one replicate reactor was characterized from each pH treatment of experiments
280 containing goethite.

281 To prepare samples for XAS, we filtered well-mixed aliquots of reactor solids and fluid
282 through 0.22μm nylon membranes inside an anoxic glove box and then sealed hydrated solids
283 with the membrane between two layers of Kapton film. Anoxic integrity of samples prepared and
284 measured this way have been demonstrated in previous work (O'Loughlin *et al.*, 2003). We
285 collected X-ray absorption near edge spectra (XANES) and extended X-ray absorption fine
286 structure (EXAFS) spectra from standards and reactor solids in transmission mode using gas-
287 filled ionization chambers. Energy calibration was set to the inflection point in an iron foil
288 spectrum (7,112 eV) and was continuously maintained by collecting spectra from the foil
289 simultaneously with the data from the samples. Radiation-induced changes in the spectra were
290 not detected and no differences were observed between spectra from fresh areas on the sample,
291 so all scans from each sample were averaged to produce the final spectrum.

292 We quantified the average oxidation state and speciation of Fe in the samples by linear
293 combination (LC) fits of the XANES and EXAFS spectra using the program Athena (Ravel &
294 Newville, 2005). The LC analysis utilized spectra from reduced and oxidized Fe standards
295 (mackinawite, FeO, $Fe(OH)_2$, vivianite, siderite, green rust, magnetite, goethite, ferrihydrite)
296 measured previously at the same beamline (Latta *et al.*, 2012; Kwon *et al.*, 2014).

297

298 **2.6. Microbial community analysis**

We collected samples for microbial community analysis at the end of the incubation from each reactor and at the beginning of the incubation from some of the reactors. To obtain each sample, we mixed the reactors, withdrew 3 mL of reactor fluid and solids with a sterile syringe, and then filtered the slurry onto a mixed-cellulose-ester filter membrane with 0.22 μm pores. Prior to sampling, we sterilized the membranes and filter housing using an autoclave (30 minutes at 121°C). After filtering, we placed the membranes in sterile 2 mL centrifuge tubes, preserved them with 0.2 mL of sucrose lysis buffer (Giovannoni *et al.*, 1990), and stored them at −80°C.

We analyzed the samples as described previously (Marquart *et al.*, 2019). A detailed description of the analysis is available in the Supporting Information. Briefly, we extracted total community DNA from reactor samples and marsh sediment using a MoBio PowerSoil DNA isolation kit. DNA amplification sequencing was carried out at the Environmental Sample Preparation and Sequencing Facility at Argonne National Laboratory. The facility amplified 16S rRNA genes using the polymerase chain reaction (PCR) targeting the V4 region of this gene in both bacteria and archaea using the primers 515F (5′-GTGYCAGCMGCCGCGGTAA-3′) and 806R (5′-GGACTACNVGGGTWTCTAAT-3′) (Walters *et al.*, 2016). Paired-end amplicons (151×12×151 base pairs) were then sequenced by Illumina MiSeq using customized sequencing primers and procedures (Caporaso *et al.*, 2012) . Following sequencing, amplicon libraries were processed using QIIME (Caporaso *et al.*, 2012) and USEARCH (Edgar, 2010). After quality filtering, the average sequencing depth was 25,050±8,883 sequences per sample. Taxonomy was assessed using the UCLUST algorithm (Edgar, 2010) with the SILVA reference database (version 128) (Quast *et al.*, 2013). Raw sequence data collected for this study are available to download via MG-RAST (Meyer *et al.*, 2008) under project mgp89849.

2.7. Statistical analysis

We tested the significance of differences in results between reactors using unpaired t-tests with Welch's correction to avoid the assumption of equal standard deviation between groups. To test the significance of correlations between parameters, we used Spearman's rho rank correlation tests. We carried out statistical calculations using Prism GraphPad, version 6.00 (GraphPad Software). We used two-tailed tests and considered *P*-values <0.05 to be significant.

3. RESULTS

3.1. Reactor chemistry

3.1.1. Effluent and gas

The chemical composition of reactor effluent (i.e., solution removed each week) differed considerably between experiments, reflecting the interplay between microbial activity and environmental conditions. In reactors that received pH 6.0 media, average effluent pH values initially ranged from 5.5 to 6.0 but stabilized at values ranging from 6.2 and 6.5 by day 42 (Fig. 1A; Tables SI3-7). Similarly, in reactors that received pH 7.5 media, average initial pH ranged from 6.7 to 7.3 but stabilized at values ranging from 7.5 to 8.5 by day 42.

Acetate concentrations in reactor effluent were initially higher than influent (i.e., fresh medium added each week) levels for all reactors in response to organic matter degradation in the marsh sediment. Maximum levels were higher in acidic reactors than corresponding alkaline reactors. Peak levels were also higher in reactors with goethite than those without. In reactors with goethite, average initial acetate levels ranged from 5.8 to 8.0 mM in acidic reactors and from 3.8 to 5.7 mM in alkaline reactors (Fig. 1B). In reactors without goethite (S-LA-NFe), initial acetate concentrations averaged 1.8 and 1.1 mM in acidic and alkaline reactors,

345 respectively. Regardless, by day 42, acetate concentrations fell to values near or below the
346 detection limit (15.8 μM) for all reactors and remained there for the rest of the incubation.
347 As acetate concentrations decreased, dissolved ferrous iron concentrations increased (Fig.
348 1C). In reactors with goethite, average ferrous iron concentrations peaked at values ranging from
349 2.87 to 3.25 mM in acidic reactors and 337 to 383 μM in alkaline reactors. In contrast, in
350 reactors without goethite (S-LA-NFe), ferrous iron concentrations peaked at 269 and 14 μM in
351 acidic and alkaline reactors, respectively. After reaching maximum levels, ferrous iron
352 concentrations gradually declined in all reactors but remained above the detection limit (1.8 μM)
353 for each reactor except the alkaline S-HA reactors. Among reactors with goethite, ferrous iron
354 concentrations decreased more rapidly for those that received sulfate (S-NA, S-LA, S-HA) than
355 those that did not (HA), regardless of pH.
356 In contrast to ferrous iron, sulfate concentrations decreased as acetate levels fell in
357 reactors that received sulfate (Fig. 1D). Concentrations fell more rapidly in alkaline reactors than
358 acidic reactors. In reactors with goethite, sulfate concentrations decreased to values near the
359 detection limit (7.4 μM) by 28 days. In response, we increased sulfate concentration in the
360 influent media of goethite-amended reactors from 1.5 mM to 2.5 mM on day 28 to prevent
361 sulfate supply from limiting sulfate reduction. After this point, sulfate concentrations gradually
362 increased. Final sulfate concentrations were about 2 mM in S-NA and S-LA reactors and about
363 1.2 mM in S-HA reactors.
364 For reactors without goethite (S-LA-NFe), sulfate concentrations followed a similar
365 pattern over time as those with goethite. However, we started the experiment about 5 weeks after
366 the other experiments. Based on results gathered during that time from the reactors with goethite,
367 we set the influent sulfate concentration at 2.5 mM from the start of the experiment to avoid the

potential for sulfate depletion. For reactors without sulfate in the influent media (HA), sulfate concentration remained below the detection limit (7.4 μM) throughout the experiment.

Although sulfate was consumed in each sulfate-bearing reactor, concentrations of dissolved sulfide remained near or below the detection limit for most of the reactors except for those without goethite (S-LA-NFe) and the alkaline S-HA reactors (Fig. 1E). In reactors without goethite, variation in sulfide levels mirrored variation in sulfate. Average sulfide concentrations peaked at just over 100 μM at nearly the same time that sulfate concentrations reached their minimum and then, as sulfate concentrations increased, sulfide concentrations decreased. In contrast, sulfide concentrations steadily increased in the alkaline S-HA reactors during the incubation, reaching a maximum of 65 μM on average.

Lastly, methane partial pressures were generally low, except for those without sulfate in the influent media (HA) (Fig. 1F; Table SI8). In those reactors, methane abundance steadily increased, reaching maximums of 16.95 and 12.52 kPa on average in the acidic and alkaline reactors, respectively, by the end of the incubation. In reactors with sulfate, methane partial pressures were highest in those that received the most acetate (S-HA), reaching maximums of 2.34 and 1.40 kPa on average in the acidic and alkaline reactors, respectively, by the end of the experiment. For all experiments, methane production was higher in acidic than alkaline reactors on average, matching the observed variation with pH in maximum acetate concentrations.

3.1.2. Sediment

Amounts of 0.5 N HCl-extractable ferrous iron in reactor sediments at the end of the incubations varied widely, ranging from about 0.43 mmol/L of reactor suspension to 5.21 mmol/L (Fig. 2). Within each experiment, extractable iron levels were higher on average for

391 reactors that received alkaline medium than those that received acidic medium. However, at the
392 level of replication of the experiments, differences in extractable iron between acidic and
393 alkaline reactors within each experiment were only significant for the goethite control
394 experiment (S-LA-NFe; $P = 0.0147$) and the sulfate control experiment (HA; $P = 0.0017$).

395 Between experiments, average 0.5 N HCl-extractable ferrous iron levels were
396 significantly higher in reactors with sulfate and goethite (S-NA, S-LA, and S-HA) than those
397 without sulfate (HA; $P \leq 0.0060$) or goethite (S-LA-NFe; $P < 0.0001$). Among reactors that
398 contained sulfate and goethite, average extractable ferrous iron levels increased with the acetate
399 content of the medium (S-NA < S-LA < S-HA). Average abundance of extractable ferrous iron
400 was significantly greater for S-HA compared to S-NA ($P < 0.0001$) and S-LA ($P < 0.0001$)
401 whereas S-NA and S-LA were not significantly different.

402 Based on LC analysis of XANES data, variation in the oxidation state of sediment iron
403 followed a similar pattern to extractable iron levels. The XANES edge position of the marsh
404 sediment inoculum and the goethite amendment align well with that of a crystalline goethite
405 standard, indicating that the iron in the reactors initially was predominantly ferric iron (Fig. SI3).
406 In reactor sediment samples collected at the end of the incubations, the proportion of ferrous iron
407 determined by LC analysis of XANES spectra ranged from 13 to 57% (Figs. 3, SI6-7). Among
408 reactors containing sulfate and goethite, the proportion of ferrous iron increased with acetate
409 supply (S-NA < S-LA < S-HA), matching the trend in extractable iron. In reactors without
410 sulfate (HA), the proportion of ferrous iron was similar to that in S-NA reactors, despite
411 differences in acetate supply (1 vs 0 mM). Compared to acidic reactors, the proportion of ferrous
412 iron in corresponding alkaline reactors was higher in experiments with sulfate (S-NA, S-LA, S-

413 HA) and lower in the sulfate control experiment (HA). Reactors without goethite (S-LA-NFe)
414 were not characterized by XANES.

415 XANES spectra collected from reactor sediments at the end of the incubations contain
416 spectral features indicative of mackinawite (Figs. SI4-5). LC analysis of the XANES and
417 EXAFS data confirms mackinawite presence in the samples and quantifies its abundance (Fig.
418 SI6-9). In reactors with sulfate and goethite, the proportion of mackinawite increased with
419 acetate supply (S-NA < S-LA < S-HA), consistent with the trend in extractable iron and iron
420 oxidation state. Based on the XANES results, the proportion of solid-phase iron existing within
421 mackinawite ranged from 9 to 48%. Based on the EXAFS results, the proportion ranged from 6
422 to 32%. In reactors with goethite but without sulfate (HA), mackinawite abundance was below
423 the detection limit (≤5%).
424

425 **3.2. Microbial community composition**

426 Our microbial community analysis reveals diverse communities potentially capable of a
427 broad range of metabolic reactions. Here we focus on the most abundant groups (≥ 0.5% avg.
428 relative abundance) that classified in *Deltaproteobacteria*, a class containing many of the
429 bacteria capable of iron and/or sulfate reduction (Kersters *et al.*, 2006; Weber *et al.*, 2006). On
430 average, 50% of the sequences from samples collected at the end of the incubations classified in
431 *Deltaproteobacteria*. Complete results are available in the Supporting Information (Table SI9).

432 The largest group of sequences overall was most closely related to *Geobacter* (Fig. 4), a
433 genus associated with iron reduction (Lovley *et al.*, 1993a; Lentini *et al.*, 2012; Hori *et al.*,
434 2015). In bioreactor samples collected at the end of the incubation, 21% of the sequences overall
435 classified within *Geobacter* compared to only 0.3% in the marsh sediment used to inoculate the

reactors. In reactors containing sulfate and goethite (S-NA, S-LA, S-HA), *Geobacter* relative abundance was significantly higher ($P \leq 0.0063$) on average in those receiving acidic media (30.5%) than alkaline media (15.9%), but varied insignificantly with the acetate content of the influent media (overall average: 25.3% in S-NA, 23.7% in S-LA, and 19.8% in S-HA). In sulfate-bearing reactors without goethite (S-LA-NFe), *Geobacter* relative abundance was 9.8% on average with insignificant variation between acidic (9.4%) and alkaline (10.1%) reactors. In reactors without sulfate but with goethite (HA), *Geobacter* relative abundance was 25.7% on average, again with insignificant variation between acidic (25.2%) and alkaline (26.2%) reactors.

Sequences also classified with several groups that include species capable of dissimilatory sulfate reduction, including *Desulfobacter* (2.9%), *Desulfotalea* (2.3%), *Desulfobulbus* (2.2%), *Desulfocapsa* (2.0%), *Desulfobacterium* (1.2%), *Desulfobacca* (0.8%), *Desulfomicrobium* (0.7%), *Desulfuromonas* (0.6%), and uncultured members of *Desulfobulbaceae* (6.6%), *Desulfuromonadales* (1.6%), *Syntrophobacteraceae* (0.7%), and *Desulfurellaceae* (0.6%) (Rabus *et al.*, 2006; Rosenberg *et al.*, 2006). In addition to sulfate reduction, some *Desulfobacterium* and *Desulfobulbaceae* species are capable of dissimilatory iron reduction (Lovley *et al.*, 1993b; Holmes *et al.*, 2004).

Sequences that classified with groups capable of sulfate reduction had an average relative abundance of 20.4% in the reactor samples collected at the end of the incubation and 5.0% in the sediment inoculum (Fig. 4). Their relative abundance was significantly lower ($P \leq 0.0005$) in reactors with sulfate and goethite (S-NA, S-LA, S-HA) that received acidic media (10.6%) than alkaline media (40.3%) but varied insignificantly with the acetate content of the influent media (overall average: 22.9% in S-NA, 24.3% in S-LA, and 23.3% in S-HA). In reactors with sulfate but without goethite (S-LA-NFe), their relative abundance was 22.3% overall with greater

459 average abundance in alkaline (29.4%) than acidic (15.3%) reactors. However, their relative
460 abundance varied considerably in replicate alkaline S-LA-NFe reactors and the difference
461 between acidic and alkaline reactors was not significant. In reactors without sulfate but with
462 goethite (HA), their relative abundance was 3.1% on average with significantly greater average
463 abundance in alkaline (4.2%) than acidic (2.0%) reactors ($P = 0.0040$).
464
465 **4. DISCUSSION**
466 **4.1. Reaction extent**
467 Variations in ferrous iron and sulfate concentrations reflect weekly sampling of reactor
468 solutions, weekly replacement of the sampled volume with unreacted media, precipitation and
469 sorption reactions, and iron and sulfate reduction. Thus, mass-balance calculations based on
470 variation in aqueous chemistry and fluid exchanges can be combined with sediment extraction
471 data to evaluate extents of iron reduction and sulfate reduction. We calculated the extent of iron
472 reduction based on changes in dissolved ferrous iron concentrations during each reaction interval
473 and the abundance of 0.5 N HCl-extractable ferrous iron at the end of the incubations. Similarly,
474 we calculated the extent of sulfate reduction based on changes in sulfate concentration during
475 each reaction interval. Our calculations assess net amounts of each reaction and do not
476 distinguish between potential dissimilatory and abiotic contributions. Our calculations follow
477 those of Bethke et al. (2011) and are described in detail in the Supporting Information.
478 The calculations illustrate the two-way interactions between pH and iron and sulfate
479 reduction. On one side of those interactions, the pH of the influent media influenced the extents
480 of iron and sulfate reduction. Iron reduction was greater in acidic reactors than corresponding
481 alkaline reactors within each experiment (Fig. 5A). Differences were significant ($P \leq 0.0007$) for

all experiments except the goethite control (S-LA-NFe). In contrast, sulfate reduction was greater in alkaline reactors than acidic reactors, but differences were only significant for those that received the most acetate (S-HA; $P = 0.0143$) (Fig. 5B). Thus, the extent of both reactions varied with pH but in opposite ways and by different amounts.

On the other side of these two-way interactions, reaction extent influenced the pH of the reactor effluent. During the incubations, the pH of the reactor effluent increased above the level of the influent media (Fig. 1) in response to proton consumption by iron and sulfate reduction. Consistent with this interpretation, the amount of pH increase varied directly with the extents of iron reduction and sulfate reduction (Fig. SI11A and SI11B).

Alongside variation in pH, the calculations demonstrate that acetate influx was also influential. Reaction extents were not significantly different between acidic no-acetate (NA) and low-acetate (LA) reactors or between alkaline no-acetate (NA) and low-acetate (LA) reactors despite differences in acetate influx (Fig. 5). However, significantly more iron and sulfate reduction occurred in acidic and alkaline high-acetate (HA) reactors relative to corresponding no-acetate (NA) and low-acetate (LA) reactors ($P \leq 0.0252$), consistent with the increase in mackinawite abundance with acetate supply observed by XANES and EXAFS. Thus, the increase in influent acetate concentration from 0 to 0.25 mM had little impact on reaction extent but the increase from 0.25 to 1 mM was influential.

Insignificant differences between no-acetate (NA) and low-acetate (LA) reactors may reflect supply of electron donors from organic matter degradation in the marsh sediment (Fig. 1). Because of that electron donor source, differences in electron donor availability between the no-acetate, low-acetate, and high-acetate (NA, LA, and HA) experiments were not as large as we intended. Despite this limitation to our study, however, more acetate was supplied to HA reactors

505 during the incubation (0.34 mmol) than LA (0.09 mmol) and NA (0 mmol) reactors and, as
506 discussed above, this difference significantly affected the extents of iron and sulfate reduction
507 (Fig. 5) and reactor mineralogy (Fig. SI6-9). Thus, the analysis provides a measure of the
508 influence of electron donor supply, if not as sensitive a measure as intended.

509 Lastly, the results show that sulfate reduction consumed more electron donor than iron
510 reduction in all reactors. Ferric and ferrous iron differ in oxidation state by a single electron. In
511 contrast, sulfate and sulfide sulfur differ by eight electrons. As such, at least 8X more ferric iron
512 needs to be reduced than sulfate for iron reduction to consume more electron donor than sulfate
513 reduction (Park *et al.*, 2009). In our reactors, the amount of ferric iron reduced was at most 3X
514 greater than sulfate reduced.

515

516 **4.2. pH and acetate supply**

517 Changes in reaction extent with pH and acetate supply equate to changes in the molar
518 ratio of iron reduction to sulfate reduction (Fe/SO_4^{2-} reduced). Among acidic reactors with
519 sulfate, the average molar ratio of iron to sulfate reduced was about 3:1 for no-acetate (S-NA)
520 and low-acetate (S-LA) reactors and 2:1 for high-acetate (S-HA) reactors (Fig. 6). Among
521 alkaline reactors, the ratio was about 1:1 for all experiments with sulfate and goethite (Fig. 6).
522 Thus, the results show that increasing pH and acetate supply both shifted the ratio in favor of
523 sulfate reduction. The change in influent pH from 6.0 to 7.5 caused a larger shift in reaction
524 proportions than the change in influent acetate concentration from 0.25 to 1 mM, indicating that
525 the ratio was more sensitive to pH than acetate concentration under the conditions tested.
526 Moreover, the results demonstrate that the impact of acetate concentration on the reaction ratio

was sensitive to pH. The ratio varied with acetate supply in the acidic reactors but not the alkaline reactors.

These results agree well with previous laboratory studies that have examined controls on iron reduction and sulfate reduction. Bethke et al. (2011) and Kirk et al. (2013) also observed a 1:1 ratio of iron reduction and sulfate reduction in alkaline (pH 7.40 and 7.15, respectively) semi-continuous bioreactors with goethite (Fig. 6). Similarly, Hansel et al. (2015) found that iron reduction and sulfate reduction were tightly linked in alkaline (pH 7-8) column reactors with variable ferric iron sources (ferrihydrite, Al-ferrihydrite, goethite, and hematite). The authors concluded that sulfur re-cycling was the dominant driver of iron reduction. Of these studies, only Kirk et al (2013) included a complementary acidic reactors (pH 5.87) for comparison. In contrast to their alkaline reactors, no sulfate reduction occurred. Although sulfate was available, only iron reduction occurred. Thus, they observed an even greater increase in iron reduction relative to sulfate reduction than we observed in our acidic reactors, possibly reflecting the lower pH and acetate levels of their acidic reactors compared to ours.

Our results are also consistent with potential mechanisms described in the Introduction. The decrease in the ratio of iron to sulfate reduction with increasing acetate supply in acidic reactors may reflect the limit of goethite surface area on iron reduction kinetics described previously (Roden, 2003, 2006). Moreover, the decrease in the ratio of iron to sulfate reduction with increasing pH may reflect an increase in ferrous iron sorption (Dixit & Hering, 2006) as well as a decrease in the free energy yield of iron reduction relative to sulfate reduction (Postma & Jakobsen, 1996; Bethke *et al.*, 2011; Jin & Kirk, 2018a).

To test the thermodynamic mechanism further, we calculated the free energy yields of acetotrophic goethite reduction and sulfate reduction (equations 1 and 2) for samples collected

on days when concentrations of all major ions were measured (days 42, 84, and 91). Our calculations followed those described previously (Bethke *et al.*, 2011) and are described in detail in the Supplementary Methods. The results indicate that iron reduction was more favorable than sulfate reduction by about 18 kJ/mol of acetate on average in acidic reactors. In alkaline reactors, however, sulfate reduction was more favorable than iron reduction by about 12 kJ/mol of acetate on average. Thus, the calculation results are consistent with the conclusion from earlier thermodynamic modeling studies that iron reduction loses its thermodynamic advantage over sulfate reduction as pH increases (Postma & Jakobsen, 1996; Bethke *et al.*, 2011; Jin & Kirk, 2018a). Full results of the calculation are available in Table SI11.

Taken together, these observations suggest that the limit of (oxyhydr)oxide surface area on iron reduction kinetics as well as impacts of pH on sorption and reaction energies may have helped cause the decrease in iron reduction relative to sulfate reduction with increasing pH. However, these mechanisms alone do not explain why iron reduction and sulfate reduction converged on a 1:1 ratio in alkaline reactors regardless of acetate availability. We hypothesize that this relationship reflects the impact of sulfate reduction on iron reduction, as discussed in the next section below.

4.3. pH and sulfate supply

Our mass-balance calculations show that more iron reduction occurred if sulfate reduction also occurred and that the effect was greater in alkaline reactors than acidic reactors. In acidic reactors, the extent of iron reduction was similar in complementary reactors with and without sulfate. Only 9% more iron was reduced in acidic S-HA reactors compared to complimentary sulfate-deficient controls (HA) (Fig. 5A). In contrast, at alkaline pH, the extent of

573 iron reduction was much greater if sulfate was available. About 47% more iron was reduced in
574 alkaline S-HA than HA reactors.
575 Previous laboratory studies that also observed more iron reduction if sulfate reduction
576 was also occurring include Li et al. (2006), Bethke et al. (2011) and Kwon et al. (2014). One
577 possible reason for this relationship is that sulfide generated by sulfate reduction (equation 2) can
578 react with ferrous iron produced by iron reduction (biotic or abiotic) and precipitate as
579 mackinawite (Berner, 1970; Luther & Rickard, 2005; Michel *et al.*, 2005):
580
581 $$Fe^{2+} + H_2S \leftrightarrow FeS(s) + 2\,H^+ \quad (4)$$
582
583 By precipitating ferrous iron, the reaction limits ferrous iron accumulation in solution and on
584 sorption sites and thus helps maintain a negative free energy change of iron reduction and limit
585 the impact of sorption (Bethke *et al.*, 2008, 2011).
586 A second possible reason for greater iron reduction when sulfate reduction occurs is that
587 sulfur cycling can drive iron reduction. By this mechanism, sulfide produced by sulfate reduction
588 abiotically reacts with (oxyhydr)oxides to produce ferrous iron and sulfur compounds with
589 intermediate oxidation states, such as elemental sulfur (S^0), polysulfides (S_n^{2-}), and thiosulfate
590 (S_2O_3) (Pyzik & Sommer, 1981; Canfield, 1989; Wan *et al.*, 2014), as shown in the following
591 example reaction with goethite:
592
593 $$FeOOH(s) + 2\,H^+ + 0.5\,H_2S \leftrightarrow 2\,H_2O + Fe^{2+} + 0.5\,S^0 \quad (5)$$
594

595 Some metal reducers and other groups can reduce or disproportionate these sulfur compounds
596 and produce sulfide, which can then reduce ferric iron again or react with ferrous iron and form
597 mackinawite (equation 4) (Thamdrup *et al.*, 1993; Nevin & Lovley, 2000; Straub & Schink,
598 2004).

599 Our XAS results demonstrate that mackinawite formed in reactors with sulfate. We do
600 not have direct evidence that sulfide reduced goethite. Sulfide reacts more slowly with goethite
601 than poorly crystalline phases, such as ferrihydrite (Canfield, 1989; Poulton *et al.*, 2004).
602 Moreover, results from reactors without sulfate (HA) demonstrate that iron reduction was not
603 dependent on sulfide oxidation. However, we cannot rule out the possibility that sulfide
604 oxidation contributed to iron reduction in reactors that received sulfate. Moreover, as discussed
605 below in section 4.4, some reactor microbial populations were indeed capable of catalyzing
606 associated reactions.

607 Contributions to iron reduction of both mechanisms, sulfide oxidation and mackinawite
608 precipitation, may depend on pH. Elemental sulfur reduction becomes more thermodynamically
609 favorable than reduction of crystalline (oxhydr)oxides at alkaline pH (Flynn *et al.*, 2014). As
610 such, metal reducers may increasingly reduce sulfur rather than (oxyhydr)oxides as pH increases,
611 and thereby help turn the sulfur cycle and indirectly reduce iron (Flynn et al., 2014). Secondly, as
612 noted earlier, sorption of ferrous iron increases with pH (Dixit & Hering, 2006), suggesting that
613 mackinawite precipitation has a greater potential to promote iron reduction at alkaline pH than
614 acidic pH. Lastly, mackinawite precipitation itself is also sensitive to pH. The reaction produces
615 two protons per mole of mackinawite, if written as above (equation 4), or one, if written in terms
616 of bisulfide (HS^-), which is most appropriate for our alkaline reactors. That proton production
617 would offset some of the proton consumption of dissimilatory (equation 1) and abiotic (equation

5) iron reduction, and thus help buffer against the increase in pH caused by (oxhydr)oxide reduction. These observations suggest, therefore, that contributions of these mechanisms to iron reduction may increase with pH, consistent with the pH dependence of the effect of sulfate availability that we observed.

If contributions of these mechanism do indeed increase with pH, they may explain why the ratio of iron to sulfate reduction fell near 1:1 in alkaline reactors, regardless of acetate supply, and exceeded 1:1 in acidic reactors (Fig. 6). As pH increases, the thermodynamic drive of (oxyhydr)oxide reduction decreases, and dissimilatory iron reduction may become increasingly reliant on benefits of mackinawite precipitation and/or it may also be increasingly displaced by abiotic reduction of iron by sulfide. Either way, iron reduction and sulfate reduction would be increasingly linked as pH increases. To test this hypothesis, more research is needed to better understand these mechanisms. In particular, we need a better understanding of the relative significance of their contributions to iron reduction and whether that varies with pH.

4.4. Potential roles of microbial populations

Our ability to isolate biotic and abiotic reactions is limited in part by the absence of sterile controls. However, sterile controls were included in previous studies that used the same reactor design and source of goethite as our study (Kirk *et al.*, 2010, 2013). The pH of their control reactors was also similar to our study and ranged from 5.7 to 7.3. No iron reduction occurred in the sterile controls of either study. Thus, the result suggests that iron reduction in our reactors was driven by microbial activity, either directly via dissimilatory iron reduction or indirectly via oxidation of sulfide produced by microorganisms.

Supporting this interpretation, our results show that relative abundances of *Geobacter* and potential sulfate reducers generally varied with the extent of iron reduction and sulfate reduction, respectively. Relative abundances of *Geobacter* were higher in reactor samples compared to the inoculum (Fig. 4), suggesting growth during the incubations. Similarly, relative abundances of potential sulfate reducers were higher in samples from reactors with sulfate compared to the inoculum. Moreover, for individual experiments, differences in relative abundance between acidic and alkaline reactors were mostly consistent with differences in reaction extent (Fig. SI10A and SI10B). Specifically, potential sulfate reducers had higher relative abundances in alkaline reactors, which hosted more sulfate reduction, and *Geobacter* had higher relative abundances in acidic reactors, where more iron was reduced. The lone exception to this result was *Geobacter* in experiment HA, as discussed below.

Enrichment of *Geobacter* and some of the sulfate-reducing taxa may reflect use of acetate as the electron donor in our aqueous media. Previous sediment bioreactor studies that also observed enrichment of *Geobacter* when acetate was provided include Lentini et al. (2012), Kirk et al. (2013), Hori et al. (2015), and Glodowska et al. (2020). Similarly, the genera *Desulfobacca*, *Desulfobacter*, and *Desulfobacterium* contain species capable of oxidizing acetate (Brandis-Heep *et al.*, 1983; Schauder *et al.*, 1986; Oude Elferink *et al.*, 1999). In our experiments, a variety of electron donors were likely supplied by degradation of organic matter in the sediment inoculum, but acetate was the primary electron donor available during most of the incubation.

In addition to dissimilatory iron and sulfate reduction, *Geobacter* and the potential sulfate reducers we detected may have also catalyzed reactions involving sulfur compounds with intermediate oxidation states. Some *Geobacter* species can respire elemental sulfur (Caccavo *et*

663 *al.*, 1994; Lovley *et al.*, 1995). Moreover, bacteria in the family *Desulfobulbaceae*, which
664 includes the genera *Desulfobulbus* and *Desulfocapsa* (Fig. 4), are capable of sulfur
665 disproportionation when ferrous iron is available to maintain low sulfide concentration (Müller *et*
666 *al.*, 2020), as was mostly the case in our reactors (Fig. 1E). *Desulfobulbaceae* species can
667 metabolize some organic compounds but none are known that can use acetate (Rabus *et al.*,
668 2006; Miletto *et al.*, 2011). Interestingly, among reactors with goethite and sulfate, the relative
669 abundance of sequences classifying in *Desulfobulbaceae* was nearly 4X higher in alkaline
670 reactors than acidic reactors. Therefore, the results show that populations capable of sulfur
671 cycling were present and that their activity may have been greater in alkaline reactors than acidic
672 reactors, consistent with our hypothesis that iron reduction by sulfide was more important in
673 alkaline reactors (section 4.3). To fully evaluate this possibility, data constraining the absolute
674 abundances of *Desulfobulbacea* and their specific function(s) would be needed.

675 Lastly, *Geobacter* may have also participated in interspecies electron transfer with
676 methanogens. In experiment HA, little iron reduction occurred in alkaline reactors and yet
677 *Geobacter* relative abundance was high (Fig. SI10a). Marquart et al. (2019) obtained similar
678 result and hypothesized that *Geobacter* responds to the lower free energy yield of goethite
679 reduction at basic pH by transferring electrons to methanogens rather than goethite. Other studies
680 that have observed high relative abundances of *Geobacter* in methanogenic systems include Hori
681 et al. (2007), Kim and Liesack (2015), Morita et al. (2011), and Rotaru et al. (2014). Our
682 taxonomic analysis revealed few methanogens (Table SI9), but we observed by far the highest
683 methane levels in HA reactors (Fig. 1F), consistent with significantly greater amounts of
684 methanogenesis in HA reactors than other reactors. Nonetheless, like the above result with

685 *Desulfobulbacea*, to fully evaluate this possibility, data constraining the absolute abundances of
686 *Geobacter* and their specific function(s) would be needed.
687
688 **4.5. Comparison to natural systems**
689 To test the environmental relevance of our experiments, we compared our results to
690 groundwater geochemistry data gathered by Kirk et al. (2016). Their analysis considered data
691 from the U.S. Geological Survey National Water Information System for 19 principal aquifers
692 distributed across the U.S., as noted previously (section 2.1). From each aquifer, they isolated
693 samples with chemistry consistent with iron and/or sulfate reducing environments based on
694 criteria for interpreting groundwater redox processes from McMahon et al. (2008). Next,
695 following the approach of Chapelle et al. (2009), Kirk et al. (2016) calculated the ratio of
696 dissolved iron to sulfide as a way to assess the proportion of iron to sulfate reduction where the
697 samples were collected. Kirk et al. (2016) calculated this ratio only for samples in their dataset
698 that had measurable concentrations of both iron and sulfide. Their dataset included 129 samples
699 that met that criteria and those samples were collected from nine different aquifers (Table SI12).
700 The calculation showed that, as pH decreases, iron/sulfide ratios increase significantly ($r = -0.43$,
701 $P < 0.0001$) (Fig. 7), consistent with an increase in iron reduction relative to sulfate reduction.
702 We compared our results to the groundwater data using ferrous iron and sulfide
703 concentrations measured at the end of the incubations in reactors with goethite and sulfate. We
704 substituted detection limit values if either ferrous iron (1.8 μM) or sulfide (1.6 μM)
705 concentration was below detection. That substitution was necessary for ferrous iron in alkaline
706 high-acetate (S-HA) reactors and for sulfide in alkaline no-acetate (S-NA) reactors.

Dissolved iron/sulfide ratios from our reactors plot within the scatter of the groundwater data and increase significantly as pH decreases ($r = -0.94$, $P = 0.0167$) (Fig. 7). Groundwater samples with data needed to calculate iron/sulfide ratios came from aquifers distributed across the U.S. (Table SI12), and thus represent a range of climate and geology. Within the aquifers, numerous factors besides rates of iron and sulfate reduction impact concentrations of ferrous iron and sulfide, including mineral precipitation, aquifer mineralogy, and sorption (Chapelle *et al.*, 2009; Kirk *et al.*, 2016). Therefore, agreement between our results and the groundwater data provides evidence that the biogeochemical relationships we observed have broad environmental relevance and can help us better understand controls on iron and sulfate reduction in natural systems.

CONCLUSIONS

The results of this study improve our ability to use pH and the supply of electron donor and acceptors to predict and manage impacts of iron reduction and sulfate reduction on environmental chemistry. We show that the molar ratio of iron to sulfate reduction increased as pH and acetate supply decreased. Under the conditions tested, the ratio between the reactions was more sensitive to pH than acetate supply. Secondly, our results demonstrate that sulfate reduction increases iron reduction. More iron was reduced in reactors with sulfate compared to control reactors without sulfate at both acidic and alkaline pH. Thirdly, our results demonstrate that the impacts of acetate and sulfate supply varied with pH. Acetate supply had a greater impact on the ratio of iron to sulfate reduction at acidic pH than alkaline pH. In contrast, sulfate availability had a greater impact on the extent of iron reduction at alkaline pH than acidic pH. Lastly, variation in the chemistry of our reactors agrees well with trends observed on a broad

scale in groundwater, providing evidence that the biogeochemical relationships we observed have strong environmental relevance and advance our understanding of controls on iron reduction and sulfate reduction in natural systems.

These findings highlight the importance of pH as a control on the proportion of iron reduction to sulfate reduction in systems that contain crystalline (oxyhydr)oxides such as goethite. Under acidic conditions, our results show that considerable iron reduction can occur independently of sulfate reduction in systems with goethite, but as pH increases, iron reduction appears to have a growing dependency on sulfate reduction, which ultimately drives the reactions toward a 1:1 ratio. The mechanisms underpinning these relationships require more attention. In particular, we need a better understanding of how the relative contributions of biotic and abiotic drivers of iron reduction shift with pH.

ACKNOWLEDGEMENTS

To be added.

CONFLICT OF INTEREST

The authors declare that there is no conflict of interest regarding the publication of this article.

ORCID

To be added.

REFERENCES

Achtnich C, Bak F, Conrad R (1995) Competition for electron donors among nitrate reducers, ferric iron reducers, sulfate reducers, and methanogens in anoxic paddy soil. *Biology and Fertility of Soils* **19**, 65–72.

Anantharaman K, Hausmann B, Jungbluth SP, Kantor RS, Lavy A, Warren LA, Rappe MS, Pester M, Loy A, Thomas BC, Banfield JF (2018) Expanded diversity of microbial groups that shape the dissimilatory sulfur cycle. *ISME Journal* **12**, 1715–1728.

Benner SG, Hansel CM, Wielinga BW, Barber TM, Fendorf S (2002) Reductive dissolution and biomineralization of iron hydroxide under dynamic flow conditions. *Environmental Science & Technology* **36**, 1705–1711.

Berner RA (1970) Sedimentary pyrite formation. *American Journal of Science* **268**, 1–23.

Bethke CM, Ding D, Jin Q, Sanford RA (2008) Origin of microbiological zoning in groundwater flows. *Geology* **36**, 739–742.

Bethke CM, Sanford RA, Kirk MF, Jin Q, Flynn TM (2011) The thermodynamic ladder in geomicrobiology. *American Journal of Science* **311**, 183–210.

Bonneville S, Behrends T, Van Cappellen P (2009) Solubility and dissimilatory reduction kinetics of iron(III) oxyhydroxides: A linear free energy relationship. *Geochimica et Cosmochimica Acta* **73**, 5273–5282.

Bonneville S, Van Cappellen P, Behrends T (2004) Microbial reduction of iron(III) oxyhydroxides: effects of mineral solubility and availability. *Chemical Geology* **212**, 255–268.

Borch T, Kretzschmar R, Kappler A, Van Cappellen P, Ginder-Vogel M, Voegelin A, Campbell K (2010) Biogeochemical Redox Processes and their Impact on Contaminant Dynamics. *Environmental Science & Technology* **44**, 15–23.

Brandis-Heep A, Gebhardt N, Thauer R, Widdel F, Pfennig N (1983) Anaerobic acetate oxidation to CO2 by Desulfobacter postgatei. I. Demonstration of all enzymes required for the operation of the citric acid cycle. *Archives of Microbiology* **136**, 222–229.

Caccavo F, Lonergan DJ, Lovley DR, Davis M, Stolz JF, McInerney MJ (1994) Geobacter sulfurreducens sp. nov., a hydrogen-oxidizing and acetate-oxidizing dissimilatory metal reducing microorganism. *Applied and Environmental Microbiology* **60**, 3752–3759.

Canfield DE (1989) Reactive iron in marine-sediments. *Geochimica et Cosmochimica Acta* **53**, 619–632.

Caporaso JG, Lauber CL, Walters WA, Berg-Lyons D, Huntley J, Fierer N, Owens SM, Betley J, Fraser L, Bauer M, Gormley N, Gilbert JA, Smith G, Knight R (2012) Ultra-high-throughput microbial community analysis on the Illumina HiSeq and MiSeq platforms. *ISME Journal* **6**, 1621–1624.

Chapelle FH, Bradley PM, Thomas MA, McMahon PB (2009) Distinguishing iron-reducing from sulfate-reducing conditions. *Ground Water* **47**, 300–305.

Chapelle FH, Lovley DR (1992) Competitive exclusion of sulfate reduction by Fe(III)-reducing bacteria: A mechanism for producing discrete zones of high-iron ground water. *Ground Water* **30**, 29–36.

Cornell RM, Schwertmann U (2003) *The Iron Oxides*, 2nd edn. Wiley-VCH, New York.

Cutting RS, Coker VS, Fellowes JW, Lloyd JR, Vaughan DJ (2009) Mineralogical and morphological constraints on the reduction of Fe(III) minerals by Geobacter sulfurreducens. *Geochimica et Cosmochimica Acta* **73**, 4004–4022.

Dixit S, Hering JG (2006) Sorption of Fe(II) and As(III) on goethite in single- and dual-sorbate systems. *Chemical Geology* **228**, 6–15.

Eaton AD, Clesceri LS, Greenberg AE (1995) *Standard Methods for the Examination of Water and Wastewater*, 19th edn. American Public Health Association, American Water Works Association, and Water Environmental Federation, Washington, DC USA.

Edgar RC (2010) Search and clustering orders of magnitude faster than BLAST. *Bioinformatics* **26**, 2460–2461.

Flynn TM, O'Loughlin EJ, Mishra B, DiChristina TJ, Kemner KM (2014) Sulfur-mediated electron shuttling during bacterial iron reduction. *Science* **344**, 1039–1042.

Giovannoni SJ, Delong EF, Schmidt TM, Pace NR (1990) Tangential flow filtration and preliminary phylogenetic analysis of marine picoplankton. *Applied and Environmental Microbiology* **56**, 2572–2575.

Glodowska M, Stopelli E, Schneider M, Lightfoot A, Rathi B, Straub D, Patzner M, Duyen VT, Berg M, Kleindienst S, Kappler A (2020) Role of in Situ Natural Organic Matter in Mobilizing As during Microbial Reduction of Fe-III-Mineral-Bearing Aquifer Sediments from Hanoi (Vietnam). *Environmental Science & Technology* **54**, 4149–4159.

Hansel CM, Lentini CJ, Tang Y, Johnston DT, Wankel SD, Jardine PM (2015) Dominance of sulfur-fueled iron oxide reduction in low-sulfate freshwater sediments. *The ISME Journal* 1–13.

Heron G, Crouzet C, Bourg ACM, Christensen TH (1994) Speciation of Fe(II) and Fe(III) in contaminated aquifer sediments using chemical-extraction techniques. *Environmental Science & Technology* **28**, 1698–1705.

Holmes DE, Bond DR, Lovley DR (2004) Electron transfer by Desulfobulbus propionicus to Fe(III) and graphite electrodes. *Applied and Environmental Microbiology* **70**, 1234–1237.

Hori T, Aoyagi T, Itoh H, Narihiro T, Oikawa A, Suzuki K, Ogata A, Friedrich MW, Conrad R, Kamagata Y (2015) Isolation of microorganisms involved in reduction of crystalline iron(III) oxides in natural environments. *Frontiers in Microbiology* **6**.

Hungate RE (1969) A roll-tube method for cultivation of strict anaerobes. *Methods in Microbiology* **3B**, 117–132.

Hunger S, Benning LG (2007) Greigite: a true intermediate on the polysulfide pathway to pyrite. *Geochemical Transactions* **8**.

Jakobsen R, Postma D (1999) Redox zoning, rates of sulfate reduction and interactions with Fe-reduction and methanogenesis in a shallow sandy aquifer, Romo, Denmark. *Geochimica et Cosmochimica Acta* **63**, 137–151.

Jin Q (2012) Energy conservation of anaerobic respiration. *American Journal of Science* **312**, 573–628.

Jin Q, Bethke CM (2007) The thermodynamics and kinetics of microbial metabolism. *American Journal of Science* **307**, 643–677.

Jin Q, Kirk MF (2018a) pH as a primary control in environmental microbiology: 1. Thermodynamic perspective. *Frontiers in Environmental Science* **6**, 1–15.

Jin Q, Kirk MF (2018b) pH as a primary control in environmental microbiology: 2. Kinetic perspective. *Frontiers in Environmental Science* **6**, 1–16.

Jorgensen BB (1982) Mineralization of organic matter in the sea bed - the role of sulfate reduction. *Nature* **296**, 643–645.

Kersters K, DeVos P, Gillis M, Swings J, VanDamme P, Stackebrandt E (2006) Introduction to the Proteobacteria. In: *The Prokaryotes* (eds. Rosenberg E, Delong EF, Lory S, Stackebrandt E, Thompson F). Springer, New York, NY, pp. 3–37.

Kim Y, Liesack W (2015) Differential assemblage of functional units in paddy soil microbiomes. *Plos One* **10**.

Kirk MF, Jin Q, Haller BR (2016) Broad-scale evidence that pH influences the balance between microbial iron and sulfate reduction. *Groundwater* **54**, 406–413.

Kirk MF, Roden EE, Crossey LJ, Brearley AJ, Spilde MN (2010) Experimental analysis of arsenic precipitation during microbial sulfate and iron reduction in model aquifer sediment reactors. *Geochimica et Cosmochimica Acta* **74**, 2538–2555.

Kirk MF, Santillan EFU, Sanford RA, Altman SJ (2013) CO2-induced shift in microbial activity affects carbon trapping and water quality in anoxic bioreactors. *Geochimica et Cosmochimica Acta* **122**, 198–208.

Konhauser KO, Kappler A, Roden EE (2011) Iron in microbial metabolisms. *Elements* **7**, 89–93.

Kropf AJ, Katsoudas J, Chattopadhyay S, Shibata T, Lang EA, Zyryanov VN, Ravel B, McIvor K, Kemner KM, Scheckel KG, Bare SR, Terry J, D KS, Bunker BA, Segre CU (2010) The new MRCAT (sector 10) bending magnet beamline at the Advanced Photon Source. Presented at the 10th International Conference on Radiation Instrumentation, American Institute of Physics, pp. 299–302.

Küsel K, Dorsch T (2000) Effect of supplemental electron donors on the microbial reduction of Fe(III), sulfate, and CO2 in coal mining-impacted freshwater lake sediments. *Microbial Ecology* **40**, 238–249.

Kwon MJ, Boyanov MI, Antonopoulos DA, Brulc JM, Johnston ER, Skinner KA, Kemner KM, O'Loughlin EJ (2014) Effects of dissimilatory sulfate reduction on FeIII (hydr)oxide reduction and microbial community development. *Geochimica et Cosmochimica Acta* **129**, 177–190.

LaRowe DE, Amend JP (2015) Catabolic rates, population sizes and doubling/replacement times of microorganisms in natural settings. *American Journal of Science* **315**, 167–203.

LaRowe DE, Dale AW, Amend JP, Van Cappellen P (2012) Thermodynamic limitations on microbially catalyzed reaction rates. *Geochimica et Cosmochimica Acta* **90**, 96–109.

Larsen O, Postma D (2001) Kinetics of reductive bulk dissolution of lepidocrocite, ferrihydrite, and goethite. *Geochimica Et Cosmochimica Acta* **65**, 1367–1379.

Latta DE, Boyanov MI, Kemner KM, O'Loughlin EJ, Scherer MM (2012) Abiotic reduction of uranium by Fe(II) in soil. *Applied Geochemistry* **27**, 1512–1524.

Lentini CJ, Wankel SD, Hansel CM (2012) Enriched iron(III)-reducing bacterial communities are shaped by carbon substrate and iron oxide mineralogy. *Frontiers in Microbiology* **3**.

Li YL, Vali H, Yang J, Phelps TJ, Zhang CL (2006) Reduction of iron oxides enhanced by a sulfate-reducing bacterium and biogenic H2S. *Geomicrobiology Journal* **23**, 103–117.

Lovley DR, Coates JD, BluntHarris EL, Phillips EJP, Woodward JC (1996) Humic substances as electron acceptors for microbial respiration. *Nature* **382**, 445–448.

Lovley DR, Giovannoni SJ, White DC, Champine JE, Phillips EJP, Gorby YA, Goodwin S (1993a) Geobacter metallireducens gen. nov. sp. nov., a microorganism capable of coupling the complete oxidation of organic-compounds to the reduction of iron and other metals. *Archives of Microbiology* **159**, 336–344.

Lovley DR, Goodwin S (1988) Hydrogen concentrations as an indicator of the predominant terminal electron-accepting reactions in aquatic sediments. *Geochimica et Cosmochimica Acta* **52**, 2993–3003.

Lovley DR, Phillips EJP (1987) Competitive mechanisms for inhibition of sulfate reduction and methane production in the zone of ferric iron reduction in sediments. *Applied and Environmental Microbiology* **53**, 2636–2641.

Lovley DR, Phillips EJP (1988) Novel mode of microbial energy metabolism: organic-carbon oxidation coupled to dissimilatory reduction of iron or manganese. *Applied and Environmental Microbiology* **54**, 1472–1480.

Lovley DR, Phillips EJP, Lonergan DJ, Widman PK (1995) Fe(III) AND S0 reduction by Pelobacter carbinolicus. *Applied and Environmental Microbiology* **61**, 2132–2138.

Lovley DR, Roden EE, Phillips EJP, Woodward JC (1993b) Enzymatic iron and uranium reduction by sulfate-reducing bacteria. *Marine Geology* **113**, 41–53.

Luther GW, Rickard DT (2005) Metal sulfide cluster complexes and their biogeochemical importance in the environment. *Journal of Nanoparticle Research* **7**, 389–407.

Marquart KA, Haller BR, Paper JM, Flynn TM, Boyanov MI, Shodunke G, Gura C, Jin Q, Kirk MF (2019) Influence of pH on the balance between methanogenesis and iron reduction. *Geobiology* **17**, 185–198.

McMahon PB, Chapelle FH (2008) Redox processes and water quality of selected principal aquifer systems. *Ground Water* **46**, 259–271.

Meyer F, Paarmann D, D'Souza M, Olson R, Glass EM, Kubal M, Paczian T, Rodriguez A, Stevens R, Wilke A, Wilkening J, Edwards RA (2008) The metagenomics RAST server - a public resource for the automatic phylogenetic and functional analysis of metagenomes. *BMC Bioinformatics* **9**.

Michel FM, Antao SM, Chupas PJ, Lee PL, Parise JB, Schoonen MAA (2005) Short- to medium-range atomic order and crystallite size of the initial FeS precipitate from pair distribution function analysis. *Chemistry of Materials* **17**, 6246–6255.

Miletto M, Williams KH, N'Guessan AL, Lovley DR (2011) Molecular analysis of the metabolic rates of discrete subsurface populations of sulfate reducers. *Applied and Environmental Microbiology* **77**, 6502–6509.

Müller H, Marozava S, Probst AJ, Meckenstock RU (2020) Groundwater cable bacteria conserve energy by sulfur disproportionation. *Isme Journal* **14**, 623–634.

Muller JB, Ramos DT, Larose C, Fernandes M, Lazzarin HSC, Vogel TM, Corseuil HX (2017) Combined iron and sulfate reduction biostimulation as a novel approach to enhance BTEX and PAH source-zone biodegradation in biodiesel blend-contaminated groundwater. *Journal of Hazardous Materials* **326**, 229–236.

Muyzer G, Stams AJM (2008) The ecology and biotechnology of sulphate-reducing bacteria. *Nature Reviews Microbiology* **6**, 441–454.

Nevin KP, Lovley DR (2000) Potential for nonenzymatic reduction of Fe(III) via electron shuttling in subsurface sediments. *Environmental Science & Technology* **34**, 2472–2478.

O'Loughlin EJ, Kelly SD, Cook RE, Csencsits R, Kemner KM (2003) Reduction of Uranium(VI) by mixed iron(II/iron(III) hydroxide (green rust): Formation of UO2 manoparticies. *Environmental Science & Technology* **37**, 721–727.

Oude Elferink S, Akkermans-van Vliet WM, Bogte JJ, Stams AJM (1999) Desulfobacca acetoxidans gen. nov., sp, nov., a novel acetate-degrading sulfate reducer isolated from sulfidogenic granular sludge. *International Journal of Systematic Bacteriology* **49**, 345–350.

Park J, Sanford RA, Bethke CM (2009) Microbial activity and chemical weathering in the Middendorf aquifer, South Carolina. *Chemical Geology* **258**, 232–241.

Pester M, Knorr K-H, Friedrich MW, Wagner M, Loy A (2012) Sulfate-reducing microorganisms in wetlands - fameless actors in carbon cycling and climate change. *Frontiers in Microbiology* **3**.

Postma D, Jakobsen R (1996) Redox zonation: Equilibrium constraints on the Fe(III)/SO4-reduction interface. *Geochimica et Cosmochimica Acta* **60**, 3169–3175.

Poulton SW, Krom MD, Raiswell R (2004) A revised scheme for the reactivity of iron (oxyhydr)oxide minerals towards dissolved sulfide. *Geochimica et Cosmochimica Acta* **68**, 3703–3715.

Pyzik A, Sommer S (1981) Sedimentary iron monosulfides: Kinetics and mechanisms of formation. *Geochimica et Cosmochimica Acta* **45**, 687–698.

Quast C, Pruesse E, Yilmaz P, Gerken J, Schweer T, Yarza P, Peplies J, Gloeckner FO (2013) The SILVA ribosomal RNA gene database project: improved data processing and web-based tools. *Nucleic Acids Research* **41**, D590–D596.

Rabus R, Hansen TA, Widdel F (2006) Dissimilatory sulfate- and sulfur-reducing prokaryotes. In: *The Prokaryotes* (eds. Dworkin M, Falkow S, Rosenberg E, Schleifer K-H, Stackebrandt E). Springer, New York, NY, pp. 659–768.

Ravel B, Newville M (2005) ATHENA, ARTEMIS, HEPHAESTUS: data analysis for X-ray absorption spectroscopy using IFEFFIT. *Journal of Synchrotron Radiation* **12**, 537–541.

Roden EE (2003) Fe(III) oxide reactivity toward biological versus chemical reduction. *Environmental Science & Technology* **37**, 1319–1324.

Roden EE (2006) Geochemical and microbiological controls on dissimilatory iron reduction. *Comptes Rendus Geoscience* **338**, 456–467.

Roden EE, Edmonds JW (1997) Phosphate mobilization in iron-rich anaerobic sediments: Microbial Fe(III) oxide reduction versus iron-sulfide formation. *Archiv Fur Hydrobiologie* **139**, 347–378.

Roden EE, Kappler A, Bauer I, Jiang J, Paul A, Stoesser R, Konishi H, Xu HF (2010) Extracellular electron transfer through microbial reduction of solid-phase humic substances. *Nature Geoscience* **3**, 417–421.

Roden EE, Urrutia MM (1999) Ferrous iron removal promotes microbial reduction of crystalline iron(III) oxides. *Environmental Science and Technology* **33**, 1847–1853.

Roden EE, Zachara JM (1996) Microbial reduction of crystalline iron(III) oxides: Influence of oxide surface area and potential for cell growth. *Environmental Science & Technology* **30**, 1618–1628.

Rosenberg E, Delong EF, Lory S, Stackebrandt E, Thompson F (eds.) (2006) *The Prokaryotes*. Deltaproteobacteria and Epsilonproteobacteria, 4th edn. Springer.

Schauder R, Eikmanns B, Thauer R, Widdel F, Fuchs G (1986) Acetate oxidation to CO2 in anaerobic bacteria via a novel pathway not involving reactions of the citric acid cycle. *Archives of Microbiology* **145**, 162–172.

Schwertmann U, Cornell RM (2000) *Iron oxides in the laboratory: Preparation and characterization*, 2nd edn. Weinheim, New York.

Stookey LL (1970) Ferrozine - a new spectrophotometric reagent for iron. *Analytical Chemistry* **42**, 779–781.

Straub KL, Schink B (2004) Ferrihydrite-dependent growth of Sulfurospirillum deleyianum through electron transfer via sulfur cycling. *Applied and Environmental Microbiology* **70**, 5744–5749.

Stumm W, Morgan J (1996) *Aquatic Chemistry: Chemical Equilibria and Rates in Natural Waters*. John Wiley and Sons, Inc., New York.

Thamdrup B, Finster K, Hansen JW, Bak F (1993) Bacterial disproportionation of elemental sulfur coupled to chemical reduction or iron or manganese. *Applied and Environmental Microbiology* **59**, 101–108.

Urrutia MM, Roden EE, Zachara JM (1999) Influence of aqueous and solid-phase Fe(II) complexants on microbial reduction of crystalline iron(III) oxides. *Environmental Science & Technology* **33**, 4022–4028.

Walters W, Hyde ER, Berg-Lyons D, Ackermann G, Humphrey G, Parada A, Gilbert JA, Jansson JK, Caporaso JG, Fuhrman JA, Apprill A, Knight R (2016) Improved Bacterial 16S rRNA Gene (V4 and V4-5) and Fungal Internal Transcribed Spacer Marker Gene Primers for Microbial Community Surveys. *mSystems* **1**.

Wan M, Shchukarev A, Lohmayer R, Planer-Friedrich B, Peiffer S (2014) Occurrence of Surface Polysulfides during the Interaction between Ferric (Hydr)Oxides and Aqueous Sulfide. *Environmental Science & Technology* **48**, 5076–5084.

Weber KA, Achenbach LA, Coates JD (2006) Microorganisms pumping iron: anaerobic microbial iron oxidation and reduction. *Nature Reviews Microbiology* **4**, 752–764.

Figure captions

Figure 1. Variation with time in (a) pH and concentrations of (b) acetate, (c) ferrous iron, (d) sulfate, and (e) sulfide in reactor effluent and (f) methane partial pressure in reactor headspace. Experiments were carried out in triplicate. Scatter data plot mean values. Error bars show standard deviation. Dotted horizontal lines show influent levels. Influent sulfate levels were increased from 1.5 to 2.5 on day 28 (d) for all experiments except S-LA-NFe. Influent sulfate content for S-LA-NFe was 2.5 mM for the entire incubation. Also, note differences in the scale of pH 6 and pH 7.5 plots of ferrous iron concentration (c). Data plotted are available in the Supporting Information (Tables SI3-8).

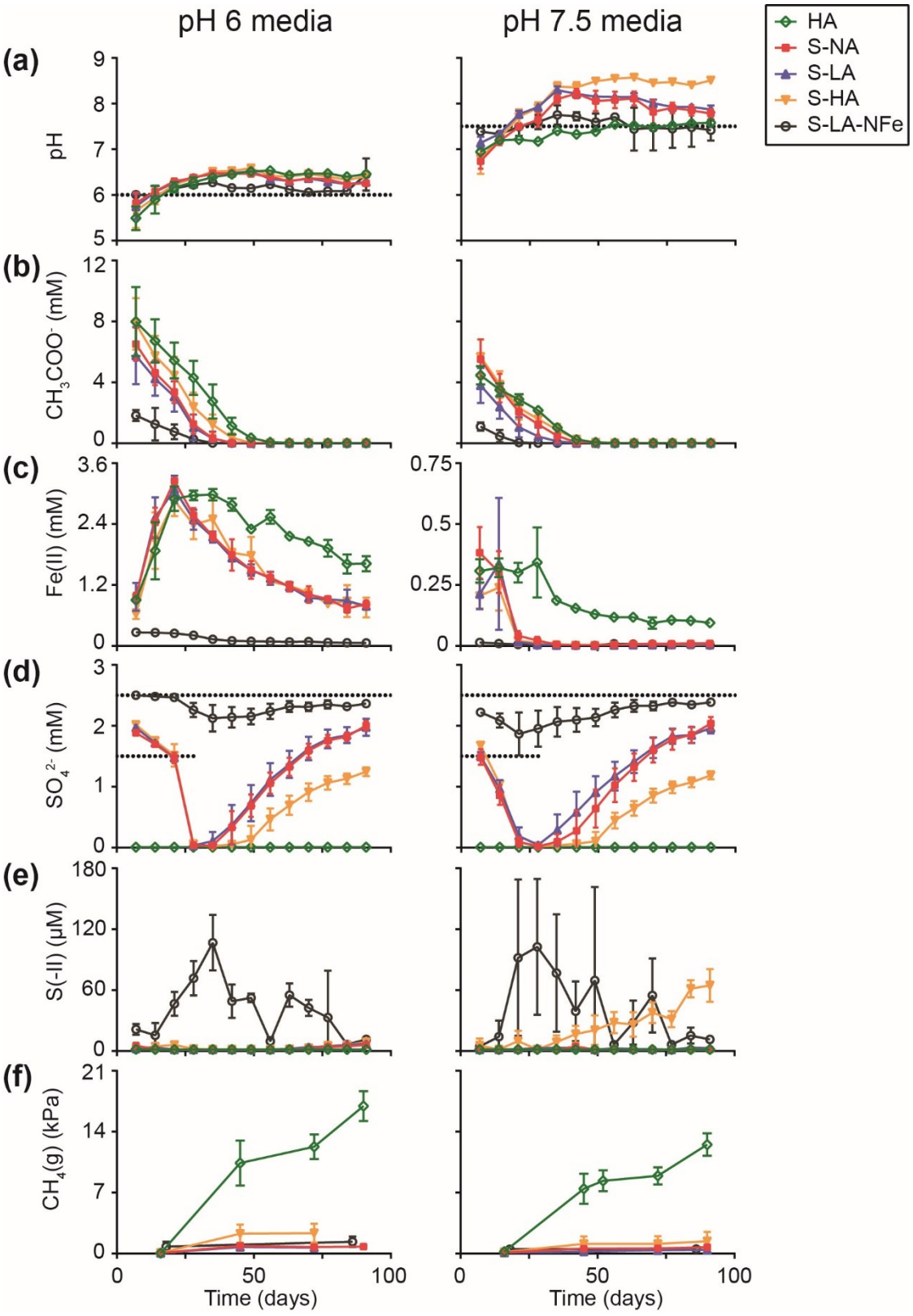
pH 6 media
pH 7.5 media
HA
S-NA
S-LA
S-HA
S-LA-NFe
(a)
pH
(b)
CH3COO- (mM)
(c)
Fe(II) (mM)
(d)
SO4 2- (mM)
(e)
S(-II) (μM)
(f)
CH4(g) (kPa)
Time (days)
Time (days)

992

993 Figure 2. Amount of 0.5 N HCl-extractable ferrous iron in reactor solids at the end of the
994 incubations. Bars show mean values for triplicate reactors and error bars show standard
995 deviation. Data plotted are available in the Supporting Information.
996

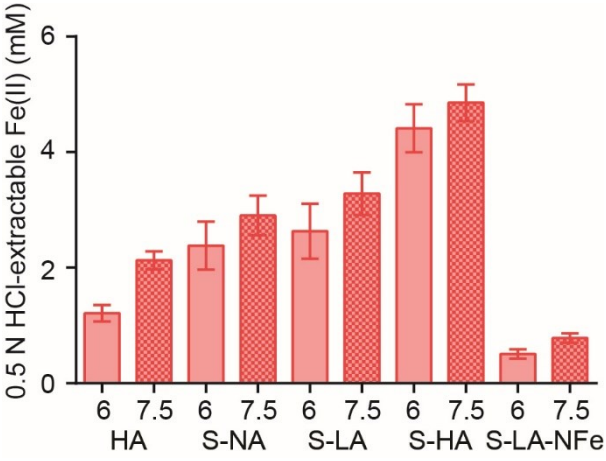

997
998

Figure 3. Proportion of ferrous iron to total solid-phase iron in reactor sediment at the end of the incubations based on LC fits of the iron K-edge XANES data. Bars depict values measured from individual samples and error bars show uncertainty associated with the analysis (7%). Experiment S-LA-NFe reactors was not included in the analysis. Details on the LC analysis can be found in Figs. SI6 and SI7.

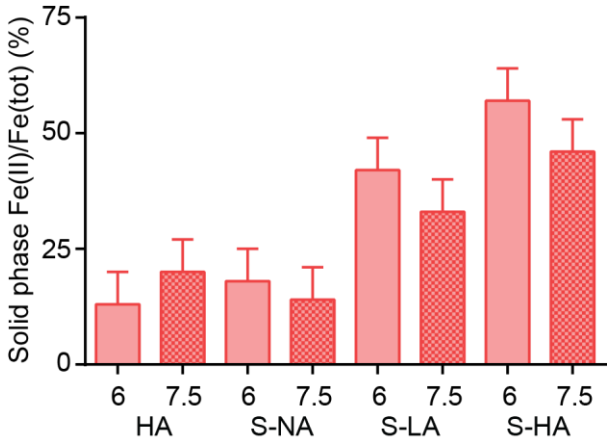

Figure 4. Relative abundances (%) of 16S rRNA gene sequences classifying in operational taxonomic units (OTUs) within class Deltaproteobacteria. Results are only shown for OTUs that had >0.5% relative abundance on average in samples collected at the end of the incubation. Results for replicate bioreactors are averaged. Complete results of our taxonomic analysis are available in the Supporting Information (Table SI9).

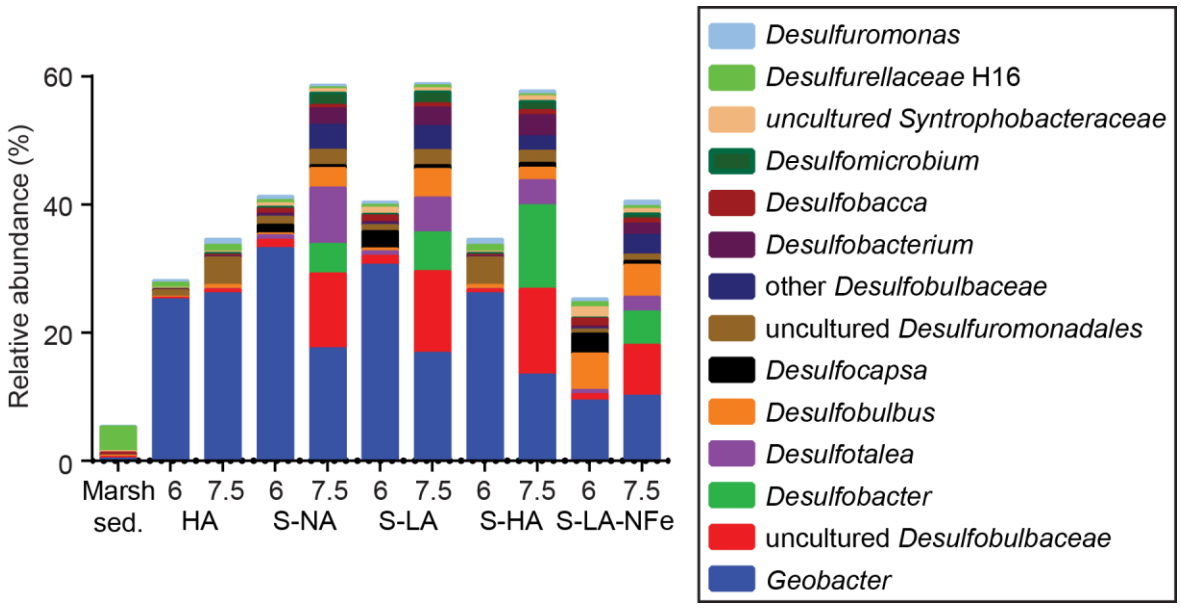

Figure 5. Total amount of (a) iron reduction and (b) sulfate reduction that occurred during the incubations based on mass-balance calculations. Bars show mean values for triplicate reactors and error bars show standard deviation. Data plotted are available in the Supporting Information (Table SI10).

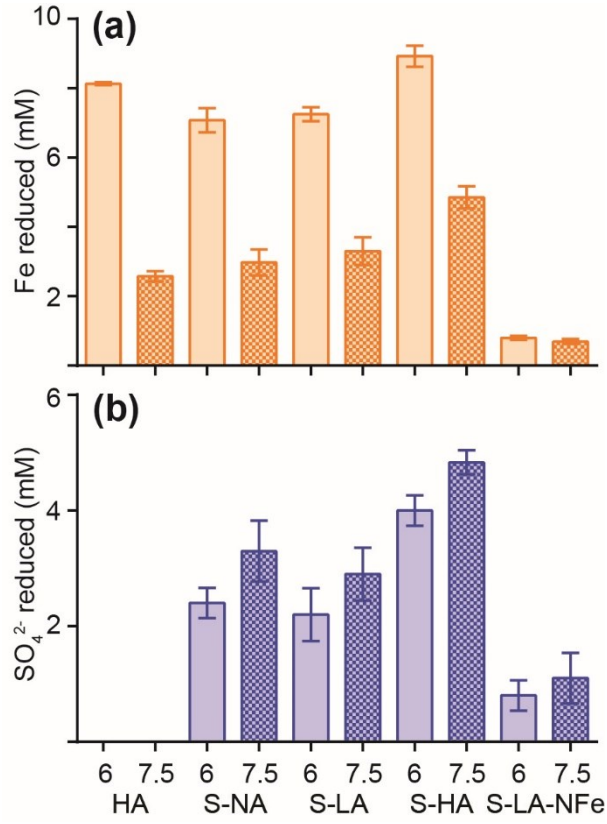

Figure 6. Variation with pH in the ratio of iron reduction to sulfate reduction. Results are shown for reactors from this study that contained goethite and sulfate as well as two previously published studies (Bethke *et al.*, 2011; Kirk *et al.*, 2013), which used a similar experimental design to ours and included goethite. For those studies, we calculated the ratio of iron reduction to sulfate reduction using their published data and the same mass-balance approach used here. The acidic bioreactors from Kirk et al. (2013) hosted no sulfate reduction and thus could not be included in this plot. Error bars show standard deviation among replicate reactors. The dashed lines and arrows highlight differences in reaction ratio trends between acidic and alkaline systems.

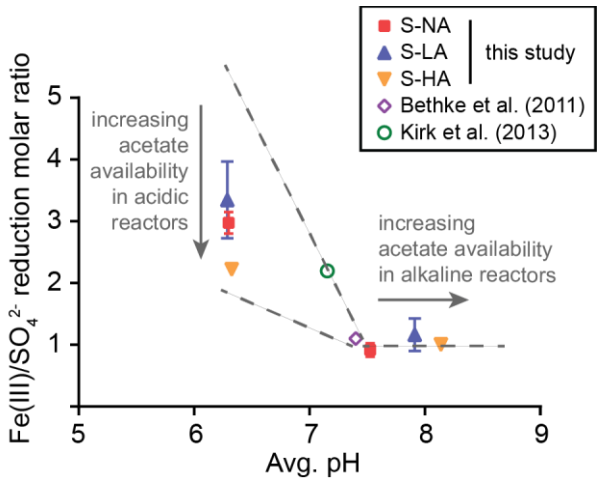

Figure 7. Variation with pH in the molar ratio of dissolved ferrous iron to sulfide (Fe(II)/S(-II)) in bioreactors and groundwater from U.S. principal aquifers. The groundwater data was isolated by Kirk et al. (2016) from the U.S. Geological Survey National Water Information System. Bioreactor values plotted are averages among replicates for concentrations measured in reactor solutions at the end of the incubations. Error bars show standard deviation. Only those reactors that received sulfate are included.